Agonist-selective recruitment of engineered protein probes and of GRK2 by opioid receptors in living cells

Miriam Stoeber[1,2*], Damien Jullié[1], Joy Li[1], Soumen Chakraborty[3,4], Susruta Majumdar[3,4], Nevin A. Lambert[5], Aashish Manglik[6,7], and Mark von Zastrow[1,8*]

[1]Department of Psychiatry, University of California San Francisco, San Francisco, CA 94143, USA. [2]Department of Cell Physiology and Metabolism, University of Geneva, 1211 Geneva, Switzerland. [3]Center for Clinical Pharmacology, Washington University School of Medicine, St. Louis, MO 63110, USA. [4]St Louis College of Pharmacy, St. Louis, MO 63110, USA. [5]Department of Pharmacology and Toxicology, Medical College of Georgia, Augusta University, Augusta, GA 30912, USA. [6]Department of Pharmaceutical Chemistry, University of California San Francisco, San Francisco, CA 94143, USA. [7]Department of Anesthesia, University of California San Francisco, San Francisco, CA 94143, USA. [8]Department of Cellular and Molecular Pharmacology, University of California San Francisco, San Francisco, CA 94143, USA.
*Corresponding authors: miriam.stoeber@unige.ch, mark@vzlab.org

Abstract

G protein-coupled receptors (GPCRs) signal through allostery, and it is increasingly clear that chemically distinct agonists can produce different receptor-based effects. It has been proposed that agonists selectively promote receptors to recruit one cellular interacting partner over another, introducing allosteric 'bias' into the signaling system. However, the core underlying hypothesis - that different agonists drive GPCRs to engage different cytoplasmic proteins in living cells - remains untested due to the complexity of downstream readouts through which receptor-proximal interactions are typically inferred. Here we describe a scalable cell-based assay to overcome this challenge, based on the use of engineered GPCR-interacting proteins as orthogonal biosensors that are disconnected from endogenous transduction mechanisms. Focusing on opioid receptors, we directly demonstrate differences between protein probe recruitment produced by chemically distinct opioid ligands in living cells. We then show how the selective recruitment applies to GRK2, a biologically relevant opioid receptor regulator protein, through discrete interactions of GRK2 with receptors or with G protein beta-gamma subunits which are differentially promoted by agonists.

Introduction

G protein-coupled receptors (GPCRs) comprise nature's largest family of signaling receptors and an important class of therapeutic drug targets. GPCRs signal by allostery, and were considered for many years to operate as binary switches that bind to cognate transducer and regulator proteins in a single agonist-induced activated state. Over the past decade an expanded view has taken hold, supported by accumulating *in vitro* evidence that GPCRs are conformationally flexible [1–5] and a confluence of cell biological and *in vivo* evidence supporting the existence of functionally selective agonist effects [6–8]. According to this still-evolving view, agonists have the potential to promote GPCRs to selectively recruit one transducer or regulator protein over another, introducing bias into the signaling cascade at a receptor-proximal level that is either propagated downstream or eliminated during intermediate transduction steps [9,10].

Opioid receptors provide a representative example. Interest in selective opioid agonist effects dates back to the initial demonstration that opioid receptors can be activated by diverse peptide and non-peptide agonists [11]. Early experimental evidence for such selectivity emerged from the detection of an agonist-induced state of opioid receptors in intact neuroblastoma cells that binds alkaloid but not peptide agonists [12]. This was followed by the demonstration of agonist-selective control of opioid receptor endocytosis, leading to recognition of functional selectivity in receptor engagement of G protein relative and beta-arrestin-dependent cellular pathways [13–16]. This concept further evolved to the present view of biased receptor recruitment of G protein relative to arrestin, with receptor-proximal selectivity calculated by fitting quantitative determinations of downstream pathway or protein readouts to operational models of receptor-effector coupling [17].

Two key gaps persist in our present understanding. First, selective protein recruitment by GPCRs in intact cells remains largely calculated rather than directly observed. Accordingly, the understanding of receptor-proximal agonist bias is inherently limited by assumptions of the model used to calculate it [18,19]. Indeed, and despite intense efforts motivated by therapeutic interest in biased agonist effects at opioid receptors [15,17], significant challenges remain in reliably assessing selectivity of receptor-proximal protein recruitment based on downstream cell-based readouts [20]. Second, challenges can arise even using cell-based assays that are direct. For example, multiple methods have been developed to detect GPCR interaction with beta-arrestins in intact cells [21,22]. However, this binding involves multiple biochemical steps and, in particular, it typically requires the receptor to undergo prior agonist-induced phosphorylation [23–25]. This has been clearly established for opioid receptors [13,26], for which strong interaction with beta-arrestin requires the receptor to be phosphorylation at multiple sites in the cytoplasmic tail through a defined sequence

of agonist-dependent reactions which are catalyzed by distinct GPCR kinase (GRK) isoforms [10,27–29]. Accordingly, beta-arrestin recruitment measured in such assays clearly reflects a process that is considerably more complex than allosteric selection by the receptor.

Here we describe an alternative approach to address these knowledge gaps. We delineate a cell-based method to simply assess selective protein recruitment by opioid receptors at the receptor-proximal level, taking advantage of two engineered protein biosensors established to bind agonist-activated GPCRs in intact cells without requiring or engaging other known cellular proteins [30,31]. Using these engineered proteins comparatively as orthogonal receptor-interaction probes, we directly demonstrate selectivity in receptor-proximal protein recruitment elicited by various opioid agonists in living cells. We then show how the principle of receptor-proximal protein selection applies in a more complex manner to GRK2, a biologically relevant regulator.

Results

Comparative detection of direct protein recruitment by opioid receptors in living cells

Two agonist-activated opioid receptor complexes have been described in structural detail (**Figure 1A**), one bound to a nucleotide-free G protein heterotrimer and another to an active state-stabilizing nanobody (Nb) [32,33]. The receptor conformation resolved in each complex is similar but not identical, with Nb and G protein interactions involving distinct molecular contacts on cytoplasmic domains of the receptor. Nbs are inherently orthogonal to intracellular biochemistry but heterotrimeric G proteins engage multiple cellular proteins in addition to activated receptors. Thus we focused on mini-G (mG) proteins, engineered versions of the Ras-like domain of G protein alpha subunits which bind directly to activated GPCRs but are not known to engage other cellular proteins [31,34]. We assessed binding to receptors in intact cells by redistribution of fluorescently labeled Nb or mG fusion proteins from the cytoplasm to the plasma membrane (**Figure 1B**).

For a mG probe we chose mGsi, derived from the Ras-like domain of Gs alpha but with 9 residues at the distal C-terminus replaced by the corresponding residues from Gi1. These C-terminal residues form a major determinant of G protein coupling specificity [35] by folding into a helical structure (alpha-5 helix) that occupies the agonist-activated GPCR core [32,36]. Because Gs couples poorly to opioid receptors, we reasoned that a sensor derived from mGsi would primarily detect this interaction. For a Nb probe we selected Nb33, previously used to detect activated mu (MOR) and delta (DOR) opioid receptors in living cells [30]. Nb33 shares receptor contact residues with

Nb39, a close variant that has been resolved at high resolution in complex with both activated MOR and KOR [33,37]. Because cytoplasmic residues contacted by the Nb in these structures are largely distinct from those engaged by the G protein alpha-5 helix, we reasoned that the Nb-derived sensor has the potential to provide different allosteric information.

Fluorescent protein fusions of mGsi or Nb33 localized diffusely when expressed in the cytoplasm of HEK293 cells, and recruitment by receptors was monitored using total internal reflection fluorescence microscopy (TIR-FM) in cells co-expressing Flag-tagged KOR (**Figure 1C**). Importantly, HEK293 cells do not express endogenous opioid receptors or other opioid ligand binding sites, thereby providing a null genetic background on which to directly examine protein probe recruitment mediated specifically by the co-expressed receptor. We observed rapid and robust recruitment of mGsi by KOR upon application of the kappa-selective peptide agonist Dynorphin A (DynA, Dynorphin 1-17). Recruitment of mGsi was reversible because application of the high-affinity competitive KOR antagonist 5'GNTI resulted in rapid redistribution of the biosensor back to the cytoplasm (**Figure 1D**). In contrast, mGs was not detectably recruited in response to KOR activation by DynA using the same assay (**Figure 1F**), verifying assay specificity and that mGsi recruitment is driven primarily by the Gi-derived distal C-terminus. Further, we verified that agonist-induced recruitment of mGsi occurred separately from a change in surface expression of KOR, which was monitored in parallel using anti-Flag antibody (**Figure 1D**). Nb33 was also rapidly recruited in response to KOR activation by DynA using the same experimental protocol, and this recruitment was also reversible upon antagonist application and occurred without a detectable change in surface receptor expression (**Figure 1E**). Accordingly, both mGsi and Nb33 can be used as biosensors of ligand-dependent recruitment by KOR in living cells using the TIR-FM assay, and both sensors produce a reversible recruitment signal that is sufficiently robust and fast ($t_{1/2}$< 30 s) to enable reliable detection of protein recruitment without possible complications of later receptor trafficking.

We next tested two non-peptide KOR full agonists, U69593 (U69) and U50488 (U50). We generated concentration-response curves by increasing agonist concentration in a stepwise manner and then adding DynA in excess (10 μM) at the end of each series as an internal reference (**Figure 1G and 1H**). Both Nb33 and mGsi were robustly recruited in a concentration-dependent manner in response to DynA and both of the non-peptide full agonist drugs (**Figure 1I - 1K**), consistent with the previously established pharmacology of these compounds [38], but we also noted that the concentration-response relationship for mGsi recruitment was consistently left-shifted relative to Nb33. These results demonstrate that both Nb33 and mGsi are robustly

recruited by KOR after activation by peptide and non-peptide full agonists in living cells, but with a potency shift indicating that the interactions are not identical.

Agonist-selective recruitment of engineered protein probes

We then applied the same approach to investigate the effect of the alkaloid agonist etorphine (ET) on mGsi and Nb33 recruitment by KOR. ET is an opiate alkaloid drug that is structurally distinct from opioid peptides as well as from U50 and U69. ET efficaciously promotes G protein activation and signaling but has long been recognized to drive KOR internalization and phosphorylation poorly, supporting its classification as a G protein-biased agonist by operational criteria [38–40]. ET behaved as a potent but partial agonist in the mGsi recruitment assay, producing a maximum biosensor recruitment response reaching 67% of that produced by DynA (**Figure 2A and 2D**). Remarkably, ET produced little or no recruitment of Nb33 despite a robust response to DynA verified in each assay and in the same cells (**Figure 2B and 2E**). This lack of Nb33 recruitment was evident even at very high concentrations of ET (**Figure 2B and 2C**), in contrast to mGsi that was potently recruited (**Figure 2C - 2E**). Further verifying this difference, selective recruitment of mGsi relative to Nb33 was observed when the biosensors were tagged with distinct fluorophores, co-expressed, and imaged in parallel in the same cells (**Figure 2F**). Again, mGsi was potently recruited in response to ET but Nb33 was not, despite DynA producing strong recruitment of both probes and in the same cells (**Figure 2G**). These results indicate that mG and Nb probes can distinguish receptor-proximal agonist effects in intact cells.

A simple interpretation of these results is that differential probe recruitment reflects a primary allosteric effect at the level of receptor-proximal protein engagement by the agonist-activated opioid receptor. An alternative possibility is that agonists produce differential probe recruitment as a secondary consequence of agonist-selective post-translational modifications of the receptor. In particular, because agonist-induced internalization of KOR requires multi-site phosphorylation on its cytoplasmic tail, and ET is known to stimulate this phosphorylation less strongly than DynA [41], we considered the possibility that differential biosensor recruitment occurs secondarily to differential phosphorylation. To test this, we measured biosensor recruitment by a mutant KOR lacking all relevant phosphorylation sites in the cytoplasmic tail (KOR-TPD for 'total phosphorylation defective', **Figure 2H**). The pronounced difference in mGsi relative to Nb33 recruitment was still observed (**Figure 2I and 2J**). Independently verifying this, selective probe recruitment by wild type KOR was not detectably perturbed in the presence of Compound101 (**Figure 2K**), a chemical inhibitor of GRK2/3 activity known to strongly reduce KOR phosphorylation in HEK293 cells [28]. Together, these results support the hypothesis that selective

recruitment of mG relative to Nb probes occurs as a primary consequence of allosteric protein selection at the receptor, rather than a secondary effect of differential phosphorylation.

Agonist-selective probe recruitment is not restricted to KOR

We next asked if our experimental strategy can also detect differential protein recruitment by MOR. Nb33 is already known to be recruited by agonist-activated MORs [30], and we verified that this is also the case for mGsi. DAMGO, a peptide full agonist of MOR, produced rapid and robust recruitment of mGsi that was rapidly reversed by the competitive antagonist naloxone (**Figure 3A and 3B**). Similar to what was observed for recruitment of the engineered protein probes by KOR, the concentration-response relationship for recruitment of mGsi by DAMGO was left-shifted relative to Nb33 (**Figure 3C**). ET (also an agonist of MOR) promoted recruitment of both probes by MOR, and to the same maximum degree when compared to the peptide full agonist (**Figure 3C**). This contrasts with partial recruitment of mGsi and no detectable recruitment of Nb33 by KOR (**Figure 2**), indicating that differential recruitment of the engineered protein probes by opioid receptors is both agonist-dependent and receptor subtype-specific.

To expand our search, and taking into account the fact that DAMGO and ET are both generally classified as full agonists at MOR, we next examined morphine and PZM21. Both of these non-peptide drugs are partial agonists with respect to assays of G protein activation or signaling, but each is derived from a different chemical scaffold and exhibits a different degree of bias when tested using a beta-arrestin recruitment assay [42]. Using the same experimental protocol, and comparing recruitment promoted by the test ligand relative to the peptide full agonist (DAMGO) reference, both morphine and PZM21 produced partial recruitment of mGsi as well as Nb33 (**Figure 3D and 3E**). Whereas morphine and PZM21 were similar in the degree of mGsi recruitment that they produced at saturating concentration, morphine was found to be significantly more efficacious than PZM21 in recruiting Nb33. Together, these results reveal a range of differential recruitment effects among chemically diverse MOR partial agonists.

The experimental strategy used to compare test agonist effects relative to the peptide reference was robust in practice but, in principle, it could underestimate differences relative to the reference peptide if the test agonist dissociates slowly or has an on-rate much faster than the peptide reference. We found evidence for this when evaluating another chemically distinct MOR partial agonist, the semi-synthetic natural product mitragynine pseudoindoxyl (MP) [43]. Using the sequential agonist addition protocol, MP appeared to be similarly efficacious to DAMGO in promoting recruitment of mGsi because no further increase was elicited by subsequent addition

of DAMGO while, in contrast, MP failed to produce any detectable recruitment of Nb33. However, we noted that DAMGO also failed to promote recruitment of Nb33 in cells that were previously exposed to mitragynine pseudoindoxyl (**Figure 3F**), despite DAMGO promoting a strong Nb33 recruitment response in cells not previously exposed to MP (**Figure 3B**). Adding a perfusion wash step, in order to remove excess test agonist between applications, avoided this complication. With this modification, MP was verified to indeed promote mGsi recruitment by MOR, but to a significantly reduced maximal degree relative to DAMGO and without promoting detectable recruitment of Nb33 (**Figure 3G and H**). These results further expand the range of differential protein recruitment effects produced by chemically diverse MOR agonists.

Differential protein recruitment can be elicited by diverse opioid agonists

To simplify comparison across agonists and receptors, we defined the maximum recruitment response elicited by each agonist compared to the corresponding peptide full agonist reference (DynA for KOR and DAMGO for MOR) as a relative 'intrinsic activity' for each agonist (**Figure 4A**). We then plotted these relative values for each biosensor (**Figure 4B**). Some non-peptide agonists were indistinguishable from the reference peptide by this analysis, recruiting both protein probes to a similar maximal degree (corresponding to an 'I.A' value of 1 for both probes), but others departed from the diagonal. This is not consistent with the traditional concept of partial agonism based on a unitary agonist-induced receptor 'on' state, which would predict the recruitment responses elicited by all agonists to fall along the diagonal. Rather, the present results support the view that opioid receptors are more flexibly activated, enabling them to selectively recruit one interaction probe over another in living cells. They further suggest that the ability to promote selective protein recruitment is widespread among chemically diverse opioid agonists (**Figure 4C**).

Relevance to agonist-selective recruitment of GRK2

While we found the engineered biosensors useful as orthogonal probes to unambiguously assess receptor-proximal recruitment in living cells, their disconnection from endogenous cellular machineries and pathways means that they are not directly related to function. Accordingly, we next asked if agonist-selective protein recruitment applies to a physiologically relevant GPCR-interacting protein. We focused on GRK2 because this kinase is known to be important for generating agonist-selective patterns of multi-site phosphorylation in the MOR cytoplasmic tail, which convey biased effects downstream from the receptor by distinguishing engagement of beta-arrestins and regulating receptor entry into the endocytic network [10,27,30]. We were also intrigued

by GRK2 because it is recruited by activated GPCRs through multiple interactions, including with the activated GPCR and with beta-gamma subunits that are exposed on the inner membrane leaflet following activation of the G protein heterotrimer [44,45] (**Figure 5A**).

We began by examining a functional GFP-fusion of GRK2 using the same TIR-FM imaging assay used to monitor orthogonal probe recruitment. We focused on comparing the effects of ET relative to DynA on KOR because these agonist-receptor pairs appeared to differ most dramatically based on the orthogonal biosensor recruitment assay (**Figure 4**). DynA promoted rapid, concentration-dependent recruitment of GRK2 to the plasma membrane (**Figure 5B**) while ET, despite being highly potent, produced a degree of GRK2 recruitment clearly lower than that produced by DynA (**Figure 5C and D**). This difference was not a secondary effect of receptor phosphorylation because ET also produced less maximal GRK2 recruitment than DynA using the phosphorylation-defective mutant KOR-TPD in place of KOR (**Figure 5E and 5F**).

Although ET promoted recruitment of full-length GRK2 less strongly than DynA, these agonists produced similarly strong recruitment of a probe corresponding to the isolated C-terminal PH domain from GRK2 that interacts with G beta-gamma (**Figure 5G**). This suggested that GRK2 binding to G beta-gamma subunits, enabled by G protein activation triggered by either agonist, is responsible for partial recruitment promoted by ET. We independently verified this conclusion by returning to assay of full length tagged GRK2, and testing the effect of blocking Gi activation by pre-exposing cells to pertussis toxin (PTX). In this condition, ET failed to produce any detectable recruitment of GRK2. However, as expected, DynA still produced a significant recruitment response in the same cells (**Figure 5H**), but to a reduced degree relative to the recruitment response elicited by DynA in cells not previously exposed to pertussis toxin.

The above results indicate that ET and DynA share the ability to promote GRK2 recruitment to the plasma membrane via binding G beta-gamma, and that DynA engages an additional mode of binding that is separate from the G protein and not shared with ET. We hypothesized that this interaction occurs with the activated opioid receptor itself. In order to test this, we devised an assay to resolve GRK2 recruitment to the plasma membrane from GRK2 binding directly to the receptor. To do so, we clustered receptors on the cell surface using an antibody cross-linking protocol, forming clusters that appeared in TIRF images as discrete spots of laterally concentrated KOR (**Figure 6A and B**, 'KOR' panels). We then used this characteristic appearance to distinguish GRK2 recruitment to KOR-containing clusters from recruitment to the surrounding plasma membrane separately from KOR clusters. As expected, in the absence of agonist GRK2

was primarily distributed in the cytosol and not detectably associated with KOR (**Figure 6B** left, 'GRK2' panel). Within ~1 min after application of DynA, GRK2 specifically accumulated at the KOR-containing clusters (**Figure 6B** right). In contrast, application of ET produced a diffuse increase in GRK2 fluorescence at the plasma membrane but no specific accumulation at KOR-containing clusters (**Figure 6C**). Quantification of the GRK2 intensity in KOR clusters relative to the surrounding plasma membrane verified significant accumulation of GRK2 with receptors promoted by DynA but not ET (**Figure 6D**), despite both agonists promoting diffuse membrane recruitment (**Figure 5**). These results support a model of GRK2 engagement driven by discrete biochemical modes which are differentially regulated by agonists: DynA and ET share the ability to promote GRK2 recruitment to the plasma membrane via receptor-activated G beta-gamma, but DynA is different from ET in its ability to additionally promote GRK2 recruitment by binding directly to KOR (**Figure 6E**).

Discussion

The ability of agonists to impose selectively on protein recruitment by GPCRs has been proposed for many years and is a core hypothesis underlying the present concept of biased agonism [6,8,17], but testing this hypothesis in an intact cellular environment remains challenging due to the complexity of cellular transduction and regulatory pathways that GPCRs typically engage [46]. The present study describes a direct, reductionist approach to this problem based on the application of engineered proteins that bind to receptors but not other cellular proteins. We show selective recruitment of these probes by opioid receptors in living cells, and delineate how the principle of selective recruitment applies to GRK2 as a physiologically relevant regulator.

Our results indicate that selective recruitment of one cellular protein over another not only occurs in intact cells, but it is widespread and elicited by diverse agonists. All partial agonists examined were found to promote mGsi recruitment more strongly than Nb33 when present at saturating concentration. Further, concentration-response curves for mGsi relative to Nb33 recruitment by opioid receptors were left-shifted even for peptide full agonists. The allosteric nature of GPCR activation has been recognized since early studies of receptor coupling to heterotrimeric G proteins in disrupted cellular membrane fractions [47–49]. The present results are fully consistent with this concept, and expand it by providing clear biochemical evidence for discrete protein-engaged allosteric receptor states that can be selectively produced by diverse agonists in the complex environment of intact, living cells. The engineered interaction probes that we focused on here demonstrate such an additional level of allosteric selection most simply, but our results

delineating differential recruitment of GRK2 by receptors suggest that the same principle applies in a more complex manner to biologically relevant GPCR-interacting proteins.

In its present state of development, our approach is limited by the number of orthogonal probes available for assessing protein recruitment. Here we focused on two previously validated GPCR-interacting proteins, selected based on existing biophysical evidence that each recognizes different structural features of the activated receptor. It is possible, and we think likely, that still more specificity exists in receptor-proximal protein recruitment. In future studies it will be interesting to develop or adapt additional structurally diverse protein folds to address this question, and to explore additional agonist diversity using the existing probes. For example, it will be interesting to search for ligands that promote recruitment of Nb33 preferentially to mGsi.

It will also be interesting to extend the present approach to examine kinetic aspects of selective protein recruitment by receptors. We found that the orthogonal probes produce a time-invariant recruitment response within ~30 s after agonist application. This enables the presently described approach to be used as an end-point assay scalable to a drug screening platform, and we focused on steady state recruitment values in the present study for simplicity. However, in light of clear evidence for kinetic contributions to agonist-selectivity at GPCRs [19], an important future goal is to extend the present assay strategy to investigate time-dependent effects.

The specificity of protein recruitment delineated here may have broader implications because it supports the emerging view of GPCRs as allosteric machines with the potential to communicate significantly more information about local chemical environment than the mere presence or absence of a cognate agonist [50]. We propose from the present observations that the mGsi probe reports allosteric effects relevant to G protein engagement by opioid receptors, and the Nb probe reports additional effects relevant to GRK engagement. Our results support the view that biased agonism, as presently defined by operational criteria, ultimately can be deconvolved into discrete receptor-proximal selection events. The present study makes initial inroads toward decoding this underlying ‘machine language’ of GPCR signaling, and thus toward precisely delineating how much chemical information content receptors actually convey in intact cells.

Acknowledgements

Imaging experiments were carried out in the UCSF Nikon Imaging Center directed by DeLaine Larsen. We thank the group of Jean Braun at the German Research Center for Geosciences for a short-term stay of M.S. The study was supported by research grants from the NIH (DA010711 and DA012864 to M.vZ., OD023048 to A.M., and GM130142 to N.A.L.). M.S. is supported by the Swiss National Science Foundation (P300PA_164712 and PCEFP3_181282). A.M. is supported by the Searle Scholars Program.

Author Contributions

M.S. and M.vZ. conceived the experiments and wrote the manuscript. M.S., D.J., and J.L. performed the experiments and analyzed the data. S.C., S.M., N.L. and A.M. provided essential reagents and comments on the manuscript.

Declaration of Interests

The authors declare no competing interests.

Figure 1

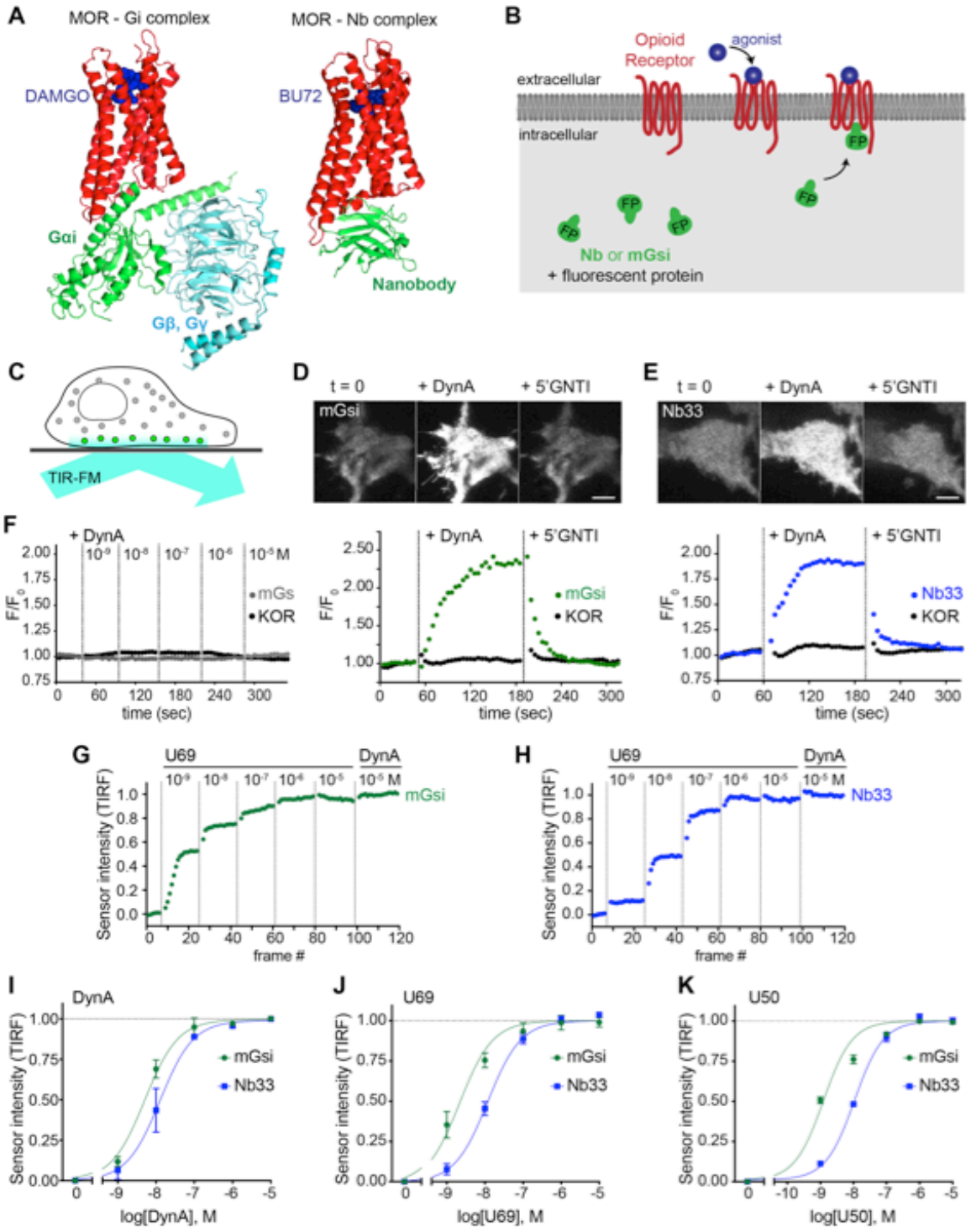

Figure 1. Comparative detection of direct probe recruitment by opioid receptors in living cells

(A) Crystal structures of the DAMGO-bound MOR (red) - Gi (green/blue) complex (PDB: 6DDF) and the BU27-bound MOR (red) – nanobody (green) complex (PDB: 5C1M). Ligands are shown

in blue. **(B)** Schematic of nanobody (Nb) / miniGsi (mGsi) and OR localization in cells and expected probe re-localization upon agonist addition. **(C)** Scheme of a cell imaged by a total internal reflection fluorescence microscopy (TIR-FM). The evanescent excitation field selectively illuminates fluorophores close to the plasma membrane. **(D)** TIR-FM images of a time series of a HEK293 cell, expressing Venus-mGsi and FLAG-KOR (not shown). Medium was exchanged to DynA (agonist, 100 nM) and to 5'GNTI (antagonist, 100 µM) by bath application. The scale bar represents 10 µm. Intensity of mGsi and KOR (labeled with anti-FLAG M1-AF647) during the TIR-FM time-lapse. 5 s between frames is shown. F_0, average fluorescence intensity before agonist. **(E)** Same as in (D) but with HEK293 cell expressing EGFP-Nb33 instead of mGsi. Intensity of Nb33 and KOR during TIR-FM time-lapse with 5 s between frames is shown. **(F)** Intensity of mGs and KOR (labeled with anti-FLAG M1-AF647) during the TIR-FM time-lapse, adding increasing concentrations of DynA (1 nM - 10 µM). 5 s between frames is shown. F_0, average fluorescence intensity before agonist. **(G)** mGsi intensity during TIR-FM time-lapse series of a HEK293 cell, co-expressing Venus-mGsi and KOR, adding increasing concentrations of U69 (1 nM - 10 µM) followed by reference compound DynA (10 µM). 5 s between frames is shown. Intensity is normalized between 0 (no agonist) and 1 (reference compound DynA). **(H)** Same as in (F) with HEK293 cell expressing EGFP-Nb33 instead of mGsi. **(I-K)** Concentration-dependent recruitment of mGsi and Nb33 probes to KOR, measured by TIR-FM upon different agonists. Normalization of intensity values is shown (range [0–1]). Regression curves with Hill slope of 1 are shown. **(I)** DynA concentration response (n = 4; average ± SEM). **(J)** U69 concentration response, normalized to DynA (n = 3; average ± SEM). **(K)** U50 concentration response, normalized to DynA (n = 4; average ± SEM).

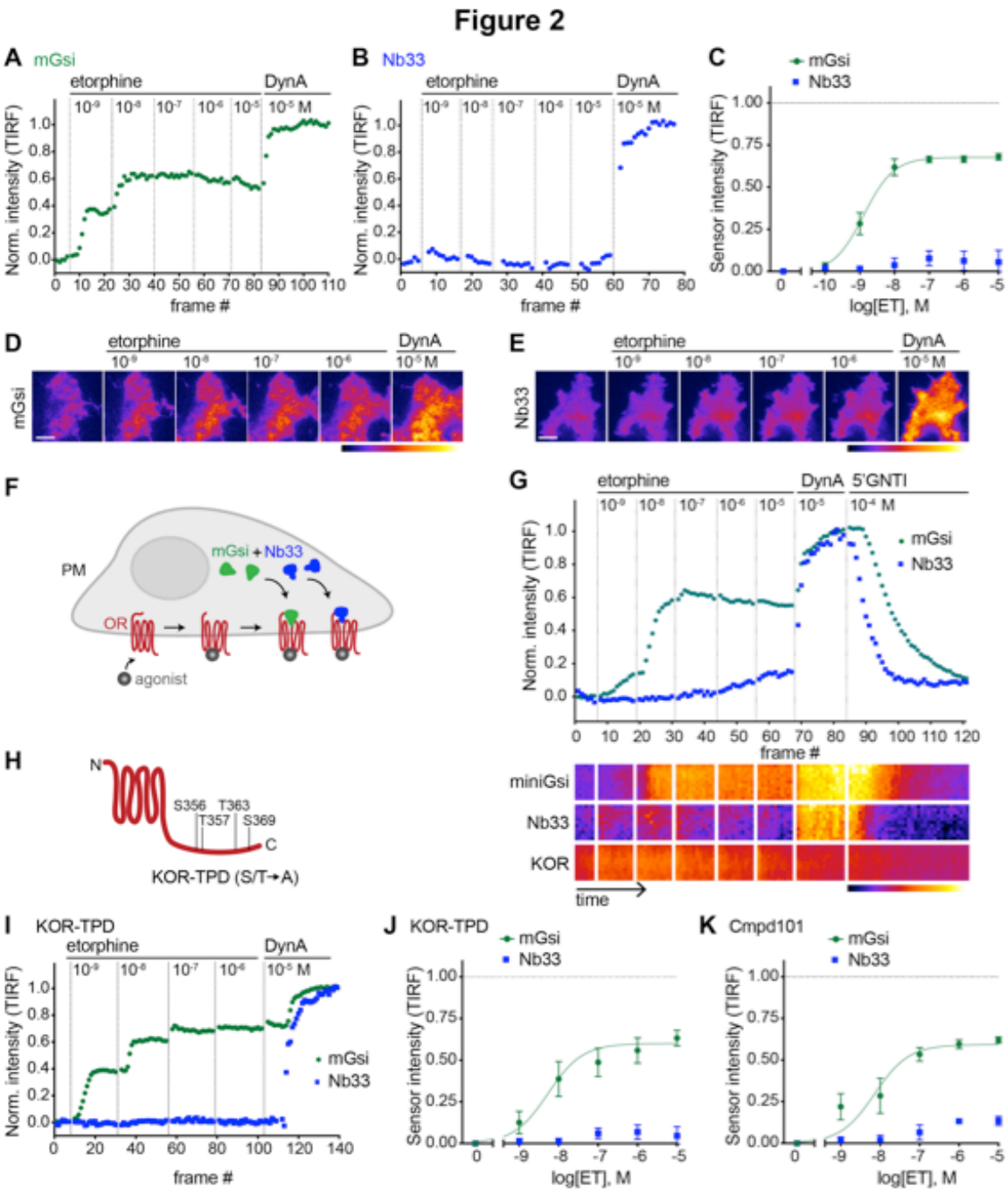

Figure 2. Selective recruitment of protein probes by KOR upon activation by etorphine
(A) mGsi intensity during TIR-FM time-lapse series of a HEK293 cell, co-expressing Venus-mGsi and KOR, adding increasing concentrations of etorphine (ET, 1 nM - 10 µM), followed by reference compound DynA (10 µM). 5 s between frames is shown. Intensity is normalized between 0 (no agonist) and 1 (reference compound DynA). **(B)** Nb33 intensity during TIR-FM time-lapse series of a HEK293 cell, co-expressing EGFP-Nb33 and FLAG-KOR, treated, imaged, and normalized as in (A). **(C)** Concentration-dependent recruitment of mGsi and Nb33 probes to KOR upon etorphine (ET) addition, measured by TIR-FM and using DynA as reference.

Normalization of intensity values is shown (range [0–1]). Regression curves with Hill slope of 1 are shown. n = 6; average ± SEM. **(D)** TIR-FM images of a time series of a HEK293 cell, expressing Venus-mGsi and KOR (not shown). Increasing concentrations of etorphine were added, followed by DynA. Venus-mGsi is pseudocolored, low to high intensity. The scale bar represents 10 μm. **(E)** Same as in (D) but with HEK293 cell expressing EGFP-Nb33 instead of mGsi. EGFP-Nb33 is pseudocolored, low to high intensity. The scale bar represents 10 μm. **(F)** Experimental set up for measuring agonist-dependent recruitment of both mGsi and Nb33 to KOR in same cell. **(G)** mGsi and Nb33 intensity during TIR-FM time-lapse series of a HEK293 cell, co-expressing Venus-mGsi, mCherry-Nb33, and FLAG-KOR. Cell was treated with increasing concentrations of etorphine, followed by DynA, and antagonist 5'GNTI. 5 s between frames is shown. Intensity is normalized between 0 (no agonist) and 1 (reference DynA). Lower panel: 10 min kymograph traced inside the cell, depicting intensities of Venus-mGsi, mCherry-Nb33, and FLAG-KOR (labeled with anti-FLAG M1-AF647), all pseudocolored, low to high intensity. **(H)** Schematic of the C-tail domain of KOR, indicating the known agonist-dependent phosphorylation sites that are mutated to alanine in KOR-TPD. **(I)** Same as in (G) but with HEK293 cell, co-expressing Venus-mGsi, mCherry-Nb33, and FLAG-KOR-TPD. **(J)** Concentration-dependent recruitment of mGsi and Nb33 probes to KOR-TPD upon etorphine addition. Experimental setup and analysis as in (C). n = 5; average ± SEM. **(H)** Concentration-dependent recruitment of mGsi and Nb33 probes to KOR upon etorphine addition, in cells pre-treated with GRK2/3 inhibitor Cmpd101 (30 μM). Experimental setup and analysis as in (C). n = 3; average ± SEM.

Figure 3

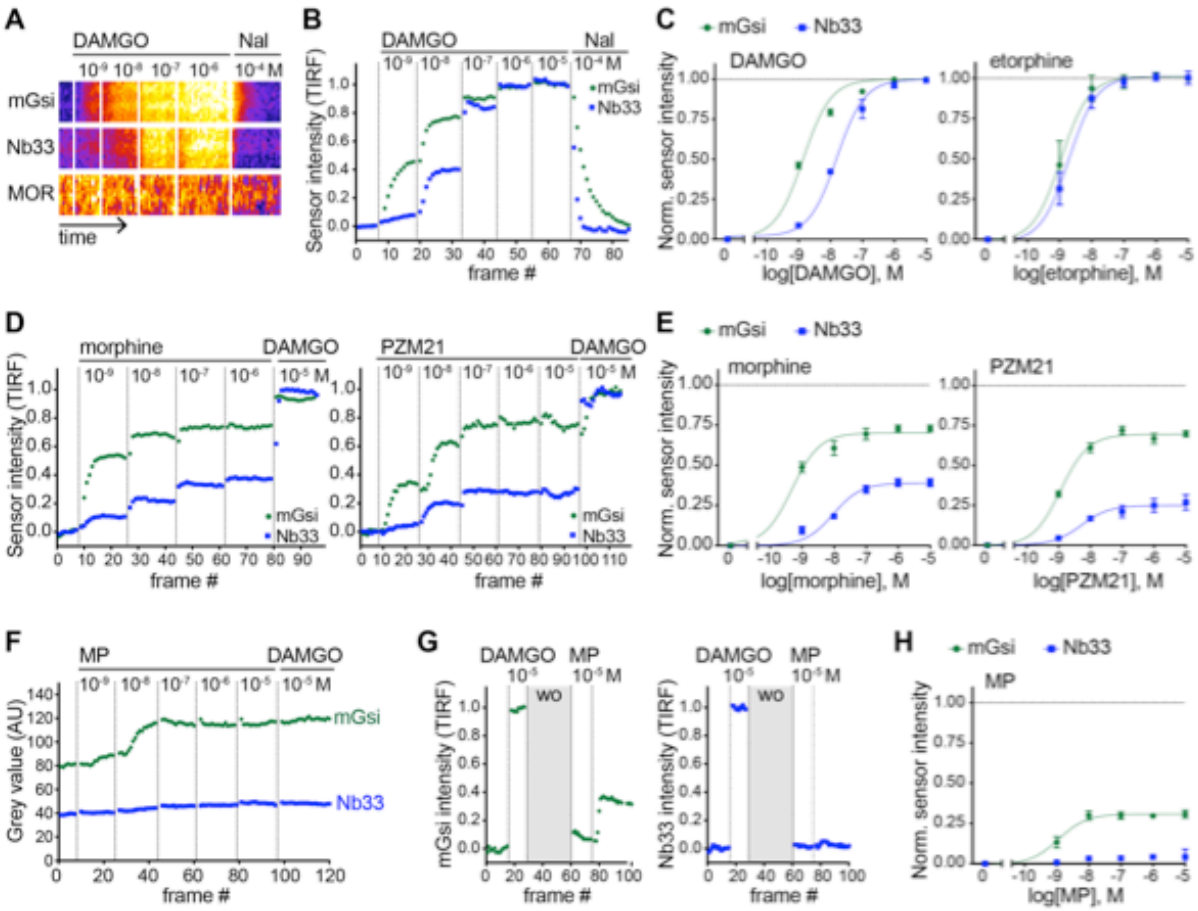

Figure 3. Agonist-selective protein probe recruitment by MOR

(A) 7 min kymograph traced inside a cell expressing Venus-mGsi, mCherry-Nb33, and FLAG-MOR (labeled with anti-FLAG M1-AF647) and treated with increasing concentrations of DAMGO (agonist), followed by addition of Naloxone (antagonist). Fluorescence intensities are pseudocolored, low to high intensity. **(B)** mGsi and Nb33 intensity during TIR-FM time-lapse series of a HEK293 cell, co-expressing Venus-mGsi, mCherry-Nb33, and FLAG-MOR, adding increasing concentrations of DAMGO followed by Naloxone. 5 s between frames is shown. Intensity is normalized between 0 (no agonist) and 1 (10 µM DAMGO). **(C)** Concentration-dependent recruitment of mGsi and Nb33 to MOR upon DAMGO and etorphine addition, measured by TIR-FM. Normalization of intensity values is shown (range [0–1]) with DAMGO as reference. Regression curves with Hill slope of 1 are shown. DAMGO n = 3, etorphine n = 4, average ± SEM. **(D)** mGsi and Nb33 intensity during TIR-FM time-lapse series of a HEK293 cell, co-expressing Venus-mGsi, mCherry-Nb33, and FLAG-MOR, adding increasing concentrations of morphine or PZM21 followed by reference compound DAMGO (10 µM). 5 s between frames is shown. Intensity is normalized between 0 (no agonist) and 1 (10 µM DAMGO). **(E)** Concentration-dependent recruitment of mGsi and Nb33 probes to MOR upon morphine or PZM21 treatment, setup and analysis as in (C). morphine n = 5, PZM21 n = 5, average ± SEM. **(F)** mGsi and Nb33 intensity during TIR-FM time-lapse series of a HEK293 cell, co-expressing Venus-mGsi, mCherry-

Nb33, and FLAG-MOR, adding increasing concentrations of mitragynine pseudoindoxyl (MP) followed by DAMGO, using bath application. 5 s between frames is shown. **(G)** mGsi (left) and Nb33 (right) intensity during TIR-FM time-lapse series of a cell, co-expressing Venus-mGsi, mCherry-Nb33, and FLAG-MOR, adding 10 µM of reference DAMGO, followed by agonist washout using perfusion ('wo', highlighted in grey), and addition of 10 µM MP. 5 s between frames is shown. Intensity is normalized between 0 (no agonist) and 1 (10 µM DAMGO). **(H)** Concentration-dependent recruitment of mGsi and Nb33 to MOR upon MP addition, measured by TIR-FM with DAMGO as reference. n = 4; average ± SEM.

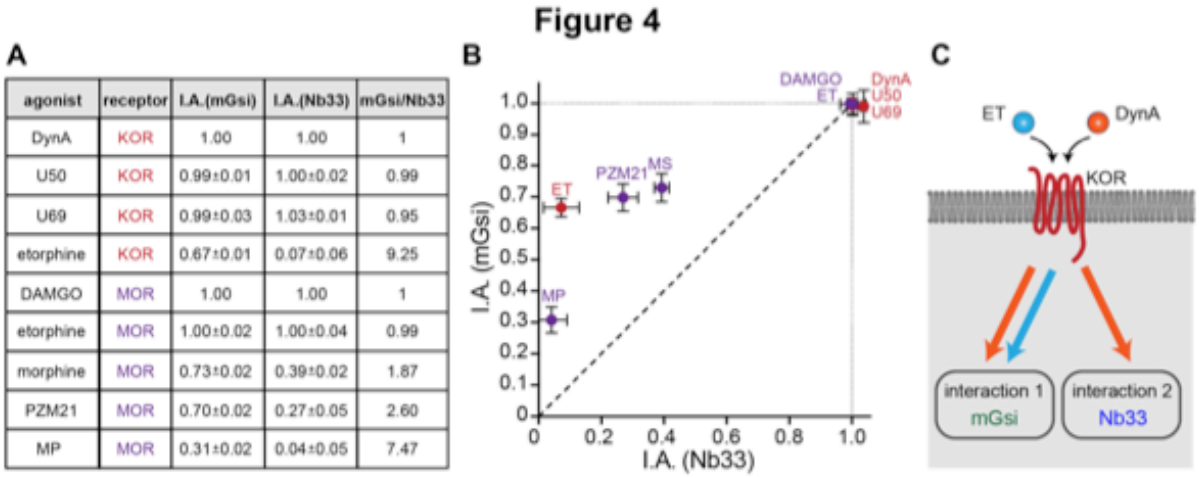

Figure 4. Receptor-proximal probe recruitment across agonists and receptors

(A) Table summarizing mGsi and Nb33 recruitment efficacies to KOR and MOR upon different agonists. Intrinsic activities ('I.A.', maximal response) for both probes and each agonist are given (average ± SEM). DynA serves as reference for KOR, DAMGO as reference for MOR. mGsi/Nb33 = ratios of intrinsic activities. **(B)** Plot of intrinsic activities (maximal responses) of mGsi recruitment as function of Nb33 recruitment for all KOR and MOR agonists. The diagonal (dotted) line indicates the theoretical trajectory for probe recruitment without bias. MS = morphine, ET = etorphine, MP = mitragynine pseudoindoxyl. **(C)** Summary of the effects of DynA vs. etorphine on KOR-proximal protein recruitment. The chemically distinct agonists differentially recruit cytoplasmic proteins mGsi (interaction 1) and Nb33 (interaction 2), suggesting that opioid receptors are able to selectively drive one interaction relative to another.

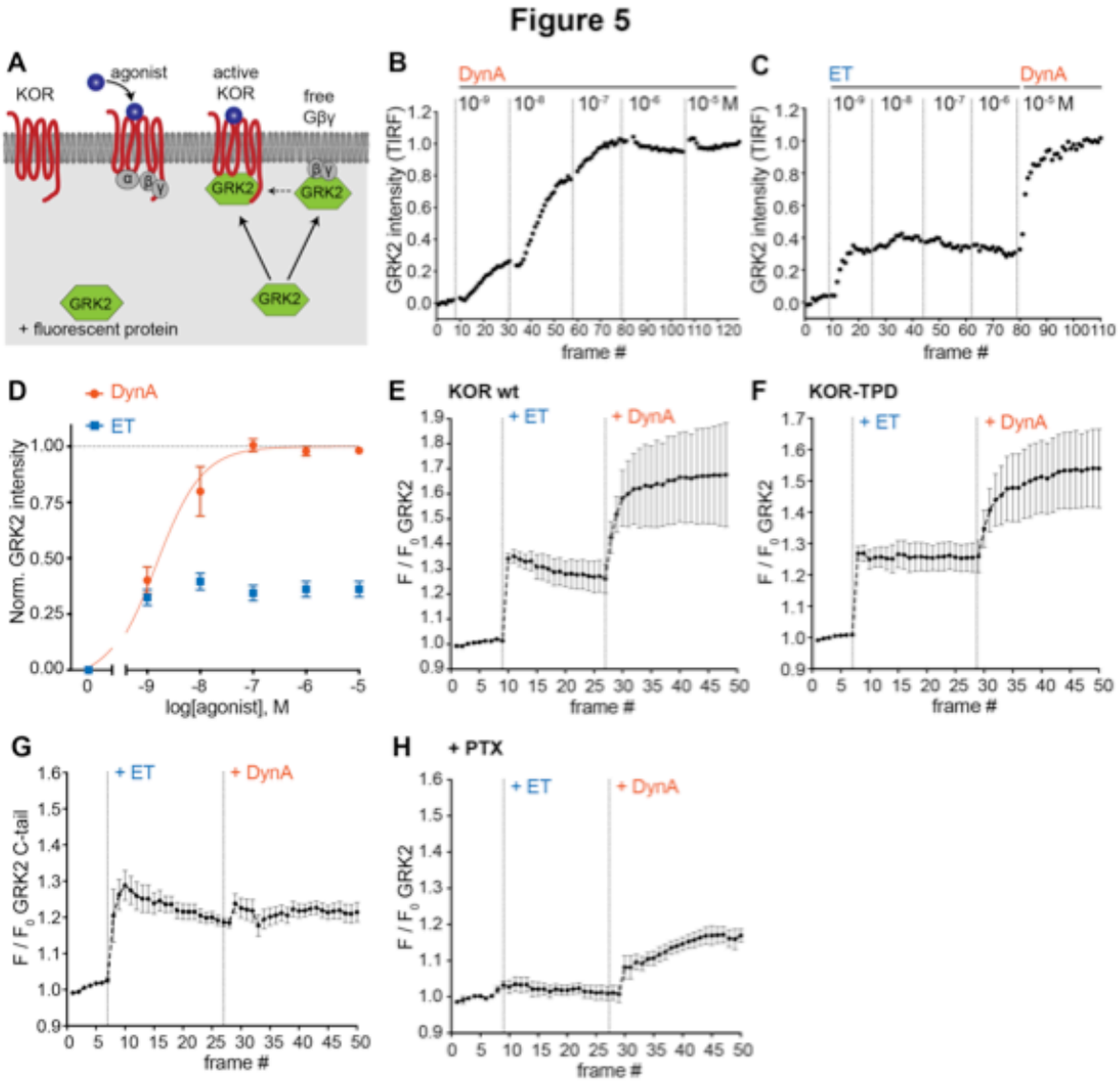

Figure 5. Agonist-selective modes of GRK2 recruitment to the plasma membrane

(A) Schematic depicting two modes of GRK2 recruitment from the cytosol to the plasma membrane upon KOR activation: one involves interaction with beta-gamma subunits exposed upon G protein activation and another with the activated receptor itself. **(B)** GRK2 intensity during TIR-FM time-lapse series of a HEK293 cell, co-expressing EGFP-GRK2 and KOR, adding increasing concentrations of DynA. 5 s between frames is shown. Intensity is normalized between 0 (no agonist) and 1 (10 µM DynA). **(C)** GRK2 intensity for cells transfected as in (B) but adding increasing concentrations of etorphine (ET), followed by 10 µM DynA as reference. Imaging and normalization as in (B). **(C)** Concentration-dependent recruitment of GRK2 to the plasma membrane upon DynA or etorphine addition, measured by TIR-FM. Normalization of intensity values is shown (range [0–1]) with DynA as reference. Regression curve with Hill slope of 1 is

shown for DynA, no fit for ET. DynA n = 6, ET n = 6, average ± SEM. **(D)** Intensity of GRK2 during the TIR-FM time-lapse series of a HEK293 cell, expressing EGFP-GRK2 and FLAG-KOR (not shown). Medium was exchanged to ET (100 nM) and then to DynA (1 µM) by bath application. 5 s between frames is shown. F_0 is the average fluorescence intensity before agonist. n = 4, average ± SEM. **(E)** GRK2 intensity time course as in (D), but cells express FLAG-KOR-TPD instead of wild-type. n = 4, average ± SEM. **(F)** Intensity of GRK2-C-tail during the TIR-FM time-lapse series of a HEK293 cell, expressing EGFP-GRK2-C-tail and FLAG-KOR, imaged and treated as in (D). n = 5, average ± SEM. **(G)** GRK2 intensity time course as in (D), but cells were pre-treated with pertussis toxin (PTX, 100 ng/ml). n = 3, average ± SEM.

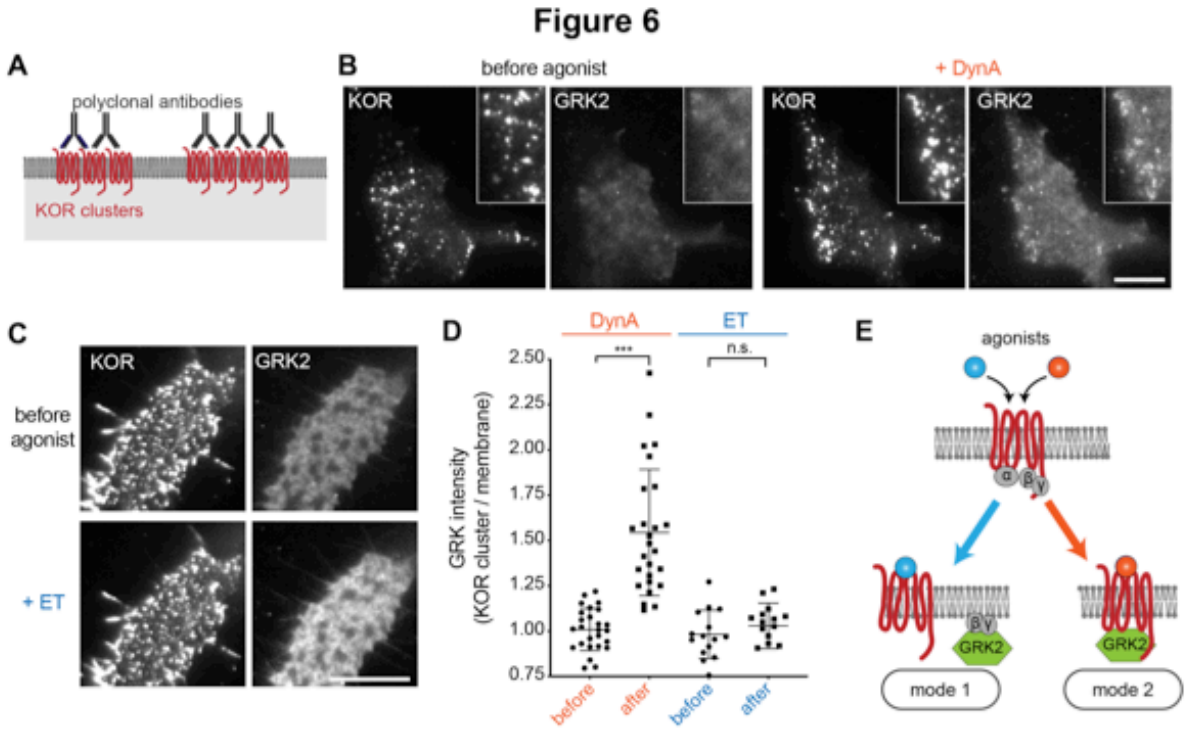

Figure 6. Agonist-selective modes of GRK2 recruitment by KOR

(A) Schematic of receptor clustering in the plasma membrane using cross-linking by polyclonal antibody. **(B)** TIR-FM images of a cell expressing mCherry-GRK2 and SEP-KOR. KOR was cross-linked with polyclonal antibodies before imaging. Frames were collected immediately before agonist (left panels) and 1 min after application of 1 μM DynA (right panels). The scale bar represents 10 μm. **(C)** Same as in (B) but cells were treated with etorphine (ET, 1 μM) instead of DynA. The scale bar represents 10 μm. **(D)** GRK2 intensity in KOR clusters relative to surrounding plasma membrane (see methods). Quantification of images collected before agonist and 2 min after agonist (DynA or ET) application, similar to images shown in (A) and (B). DynA (26 cells) and ET (15 cells) across three independent experiments. Error bars represent SEM. ***p = <0.0001 by two-tailed t-test. n.s. = not significant (p = 0.33). **(E)** The two biochemical modes of GRK2 recruitment are selectively promoted by distinct agonists. While etorphine only drives GRK2 binding to G beta-gamma, DynA additionally promotes direct interaction of GRK2 with activated KOR.

Materials and Methods

Mammalian Cell Culture Conditions

HEK293 (CRL-1573, ATCC, female)were cultured in Dulbecco's modified Eagle's medium (DMEM, GIBCO), supplemented with 10% fetal bovine serum (UCSF Cell Culture Facility). Stably transfected HEK293 cells expressing N-terminally FLAG-tagged MOR or KOR were cultured in the presence of 250 µg/ml Geneticin (Gibco). For transient DNA expression, Lipofectamine 2000 (Invitrogen) was used according to manufacturer's instructions. For live cell imaging, cells were plated on poly-L-lysine-coated 35-mm glass-bottomed culture dishes (MatTek Corporation) 48 h before the experiments. Cells were transfected 24h prior to imaging. Per 35-mm culture dish, 200 ng DNA was used for mGsi and Nb33, 300 ng DNA was used for GRK2 constructs and 1.2 µg DNA was used for receptor constructs.

cDNA constructs

GRK2-EGFP and GRK2-pmApple were created by amplifying murine GRK2 and GFP or pmApple DNA by PCR and inserting GRK2 and the respective fluorescent protein using In-Fusion cloning into pCAGGS-SE cut with KpnI and EcoRI. Super ecliptic pHluorin (SEP)-KOR was generated by PCR amplification of SEP and KOR, and insertion using In-Fusion cloning into pCAGGS-SE cut with KpnI and EcoRI.

Live cell total internal reflection fluorescence microscopy (TIR-FM)

Live cell image series measuring protein recruitment to the PM were performed at 37 °C using a Nikon Ti-E microscope equipped for through-the-objective TIR-FM with a temperature-, humidity- and CO_2-controlled chamber (Okolab), objective heater, perfect focus system, and an Andor DU897 EMCCD camera. Images were obtained with a 100x 1.49 NA Apo TIRF objective (Nikon) with solid-state lasers of 488, 561 and 647 nm (Keysight Technologies). Before imaging, receptors at the cell surface were labelled with M1 monoclonal FLAG antibody (1:1,000) conjugated to Alexa647 dye for 10 min at 37 °C. Cells were then washed and live imaged in HBS imaging solution (Hepes buffered saline (HBS) with 135 mM NaCl, 5 mM KCl, 0.4 mM MgCl2,1.8 mM CaCl2, 20 mM Hepes, 5 mM d-glucose adjusted to pH 7.4 and 300–315 mOsmol/l). Agonists or antagonists were either added by bath application at concentrations indicated in the figure legends or by media perfusion. For the latter, an insert was 3D-printed and placed inside the imaging dish where it left a dead volume of about 300 µl. It was used to perfuse FBS imaging solution with agonists or without agonists (agonist washout) at

concentrations indicated in the figure legends with a flow rate of 1.5ml/min.

Cell treatments prior to live cell imaging

To cluster receptors in the plasma membrane, cells transfected with SEP–KOR were treated with a polyclonal rabbit anti-GFP antibody (1:100) for 15 min at 37 °C. Cells were then washed and imaged live in HBS imaging solution. To inhibit GRK2/3, cells were pre-incubated with Compound101 (30 μM) for 15 min at 37 °C and Compound101 was present throughout the imaging experiment. To inhibit KOR coupling to Gai/o, cells were treated with PTX (100 ng/mL) for 16h and PTX was present throughout the imaging experiment.

Agonist concentration dependence of protein recruitment

For probing protein recruitment to the PM, HEK293 cells co-expressing the cytosolic protein of interest (mGsi, Nb33, or GRK2) and MOR or KOR were imaged using TIR-FM. Cells were treated with increasing concentrations of agonist (bath application) and imaged at a frame rate of 0.2/s (total movie length 6-8 min). Protein intensity during time lapse series was measured using ImageJ. Values were normalized between 0 (before agonist) and 1 (10 μM reference agonist). Regression curves with Hill slope of 1 were fit using Prism 8.

Quantitative image analysis

All quantitative image analysis was performed on unprocessed images using MATLAB (MathWorks, R2014b)or ImageJ (2.0.0). For quantifying mCherry-GRK2 recruitment to the plasma membrane and receptor clusters, we used a custom written MATLAB script. In brief, a polygon was drawn on the TIR-FM image to encompass the cell of interest. Then, a mask of the receptor clusters was generated by thresholding the SEP-KOR signal within the polygon. The average mCherry-GRK2 fluorescence was measured within the cluster mask (KOR clusters) and outside of the mask (membrane) of the polygon, allowing to calculate the ratio. Quantification was performed in cells imaged before (t=0) and after (t = 1-2 min) agonist addition.

Statistics

Quantification of data are presented as mean ± standard error of the mean (SEM) based on at least 3 biologically independent experiments with the precise number indicated in the figure legends. Statistical analysis was performed using Prism (8.1.1, GraphPad) and using unpaired or paired two tailed Student's t test.

TABLE OF REAGENTS

REAGENT or RESOURCE	SOURCE	IDENTIFIER
Antibodies		
Mouse anti-FLAG (M1)	Sigma-Aldrich	F-3040; RRID: AB_439712
Rabbit anti-GFP	Invitrogen	A-11122; RRID: AB_221569
Chemicals and Peptides		
Dynorphin A (1-17, DynA)	Anaspec	AS-24298
U-69593 (U69)	Cayman Chemical	13255
U-50488 hydrochloride (U50)	Tocris	0495
GNTI dihydrochloride (5'GNTI)	Axon Med Chem	1226
Etorphine-HCl	NIDA	N/A
DAMGO, [D-Ala2, N-Me-Phe4, Gly5-ol]-Enkephalin acetate salt	Sigma-Aldrich	E7384
Morphine sulfate (MS)	Sigma-Aldrich	1448005
Naloxone hydrochloride dihydrate	Sigma-Aldrich	N7758
PZM21	Enamine	custom synthesis
mitragynine pseudoindoxyl (MP)	This study	N/A
Compound101 (Cmpd101)	HelloBio	HB2840
Pertussis toxin	Sigma-Aldrich	P7208

Alexa Fluor 647 Protein Labeling Kit	Thermo Fisher Scientific	A20173
Recombinant DNA		
EGFP-C1: EGFP-Nb33	[30]	N/A
EGFP-C1: pmApple-Nb33	[30]	N/A
pcDNA3: NES-Venus-mGsi	[31]	N/A
pcDNA3: NES-Venus-mGs	[31]	N/A
pcDNA3: signal sequence FLAG (ssf)-MOR, murine	[30]	N/A
pcDNA3: signal sequence FLAG (ssf)-KOR, murine	[40]	N/A
pcDNA3: ssf-KOR-TPD (S356A, T357A, T363A, S369A)	This study	N/A
SEP-KOR	This study	N/A
pCAGGS/SE: GRK2-EGFP, murine	This study	N/A
pCAGGS/SE: GRK2-pmApple, murine	This study	N/A
pCAGGS/SE: EGFP-GRK2-C-tail (aa 546-670)	This study	N/A
Software and Algorithms		
Prism	GraphPad	8.1.1
ImageJ	Imagej.net/contributors	2.0.0-rc-54/1.51g

MATLAB	MathWorks	R2014b
Excel	Microsoft	16.16.12
PyMOL	Schrödinger	v1.7.4.5
Adobe Illustrator CC	Adobe	21.0.2

References

1. Weis, W. I. & Kobilka, B. K. The Molecular Basis of G Protein-Coupled Receptor Activation. *Annu. Rev. Biochem.* **87**, 897–919 (2018).
2. Mahoney, J. P. & Sunahara, R. K. Mechanistic insights into GPCR-G protein interactions. *Curr. Opin. Struct. Biol.* **41**, 247–254 (2016).
3. Wingler, L. M. *et al.* Angiotensin Analogs with Divergent Bias Stabilize Distinct Receptor Conformations. *Cell* **176**, 468–478.e11 (2019).
4. Nygaard, R. *et al.* The dynamic process of β(2)-adrenergic receptor activation. *Cell* **152**, 532–542 (2013).
5. Lohse, M. J. & Hofmann, K. P. Spatial and Temporal Aspects of Signaling by G-Protein-Coupled Receptors. *Mol. Pharmacol.* **88**, 572–578 (2015).
6. Urban, J. D. *et al.* Functional selectivity and classical concepts of quantitative pharmacology. *J. Pharmacol. Exp. Ther.* **320**, 1–13 (2007).
7. Williams, J. T. *et al.* Regulation of μ-opioid receptors: desensitization, phosphorylation, internalization, and tolerance. *Pharmacol. Rev.* **65**, 223–254 (2013).
8. Smith, J. S., Lefkowitz, R. J. & Rajagopal, S. Biased signalling: from simple switches to allosteric microprocessors. *Nat. Rev. Drug Discov.* **17**, 243–260 (2018).
9. Tsvetanova, N. G. *et al.* G Protein-Coupled Receptor Endocytosis Confers Uniformity in Responses to Chemically Distinct Ligands. *Mol. Pharmacol.* **91**, 145–156 (2017).
10. Lau, E. K. *et al.* Quantitative encoding of the effect of a partial agonist on individual opioid receptors by multisite phosphorylation and threshold detection. *Sci. Signal.* **4**, ra52 (2011).
11. Kosterlitz, H. W. & Hughes, J. Peptides with morphine-like action in the brain. *Br. J. Psychiatry* **130**, 298–304 (1977).
12. Von Zastrow, M., Keith, D. E., Jr & Evans, C. J. Agonist-induced state of the delta-opioid receptor that discriminates between opioid peptides and opiate alkaloids. *Mol. Pharmacol.* **44**, 166–172 (1993).
13. Whistler, J. L. & von Zastrow, M. Morphine-activated opioid receptors elude desensitization by beta-arrestin. *Proc. Natl. Acad. Sci. U. S. A.* **95**, 9914–9919 (1998).
14. Keith, D. E. *et al.* Morphine activates opioid receptors without causing their rapid internalization. *J. Biol. Chem.* **271**, 19021–19024 (1996).
15. Whistler, J. L., Chuang, H. H., Chu, P., Jan, L. Y. & von Zastrow, M. Functional dissociation of mu opioid receptor signaling and endocytosis: implications for the biology of opiate tolerance and addiction. *Neuron* **23**, 737–746 (1999).
16. Keith, D. E. *et al.* mu-Opioid receptor internalization: opiate drugs have differential effects

on a conserved endocytic mechanism in vitro and in the mammalian brain. *Mol. Pharmacol.* **53**, 377–384 (1998).

17. Schmid, C. L. *et al.* Bias Factor and Therapeutic Window Correlate to Predict Safer Opioid Analgesics. *Cell* **171**, 1165–1175.e13 (2017).
18. Kenakin, T. Is the Quest for Signaling Bias Worth the Effort? *Mol. Pharmacol.* **93**, 266–269 (2018).
19. Klein Herenbrink, C. *et al.* The role of kinetic context in apparent biased agonism at GPCRs. *Nat. Commun.* **7**, 10842 (2016).
20. Conibear, A. E. & Kelly, E. A biased view of μ opioid receptors? *Mol. Pharmacol.* (2019). doi:10.1124/mol.119.115956
21. Kim, M. W. *et al.* Time-gated detection of protein-protein interactions with transcriptional readout. *Elife* **6**, (2017).
22. Chen, L., Jin, L. & Zhou, N. An update of novel screening methods for GPCR in drug discovery. *Expert Opin. Drug Discov.* **7**, 791–806 (2012).
23. Thomsen, A. R. B. *et al.* GPCR-G Protein-β-Arrestin Super-Complex Mediates Sustained G Protein Signaling. *Cell* **166**, 907–919 (2016).
24. Eichel, K. *et al.* Catalytic activation of β-arrestin by GPCRs. *Nature* **557**, 381–386 (2018).
25. Gurevich, V. V. *et al.* Arrestin interactions with G protein-coupled receptors. Direct binding studies of wild type and mutant arrestins with rhodopsin, beta 2-adrenergic, and m2 muscarinic cholinergic receptors. *J. Biol. Chem.* **270**, 720–731 (1995).
26. Zhang, J. *et al.* Role for G protein-coupled receptor kinase in agonist-specific regulation of mu-opioid receptor responsiveness. *Proc. Natl. Acad. Sci. U. S. A.* **95**, 7157–7162 (1998).
27. Just, S. *et al.* Differentiation of opioid drug effects by hierarchical multi-site phosphorylation. *Mol. Pharmacol.* **83**, 633–639 (2013).
28. Chiu, Y.-T., Chen, C., Yu, D., Schulz, S. & Liu-Chen, L.-Y. Agonist-Dependent and -Independent κ Opioid Receptor Phosphorylation: Distinct Phosphorylation Patterns and Different Cellular Outcomes. *Mol. Pharmacol.* **92**, 588–600 (2017).
29. Miess, E. *et al.* Multisite phosphorylation is required for sustained interaction with GRKs and arrestins during rapid μ-opioid receptor desensitization. *Sci. Signal.* **11**, (2018).
30. Stoeber, M. *et al.* A Genetically Encoded Biosensor Reveals Location Bias of Opioid Drug Action. *Neuron* **98**, 963–976.e5 (2018).
31. Wan, Q. *et al.* Mini G protein probes for active G protein–coupled receptors (GPCRs) in live cells. *J. Biol. Chem.* **293**, 7466–7473 (2018).
32. Koehl, A. *et al.* Structure of the μ-opioid receptor-Gi protein complex. *Nature* **558**, 547–552

(2018).

33. Huang, W. *et al.* Structural insights into μ-opioid receptor activation. *Nature* **524**, 315–321 (2015).
34. Nehmé, R. *et al.* Mini-G proteins: Novel tools for studying GPCRs in their active conformation. *PLoS One* **12**, e0175642 (2017).
35. Conklin, B. R., Farfel, Z., Lustig, K. D., Julius, D. & Bourne, H. R. Substitution of three amino acids switches receptor specificity of Gq alpha to that of Gi alpha. *Nature* **363**, 274–276 (1993).
36. Carpenter, B. & Tate, C. G. Active state structures of G protein-coupled receptors highlight the similarities and differences in the G protein and arrestin coupling interfaces. *Curr. Opin. Struct. Biol.* **45**, 124–132 (2017).
37. Che, T. *et al.* Structure of the Nanobody-Stabilized Active State of the Kappa Opioid Receptor. *Cell* **172**, 55–67.e15 (2018).
38. DiMattio, K. M., Ehlert, F. J. & Liu-Chen, L.-Y. Intrinsic relative activities of κ opioid agonists in activating Gα proteins and internalizing receptor: Differences between human and mouse receptors. *Eur. J. Pharmacol.* **761**, 235–244 (2015).
39. Jordan, B. A., Cvejic, S. & Devi, L. A. Kappa opioid receptor endocytosis by dynorphin peptides. *DNA Cell Biol.* **19**, 19–27 (2000).
40. Chu, P., Murray, S., Lissin, D. & von Zastrow, M. Delta and kappa opioid receptors are differentially regulated by dynamin-dependent endocytosis when activated by the same alkaloid agonist. *J. Biol. Chem.* **272**, 27124–27130 (1997).
41. Chen, C. *et al.* Determination of sites of U50,488H-promoted phosphorylation of the mouse κ opioid receptor (KOPR): disconnect between KOPR phosphorylation and internalization. *Biochem. J* **473**, 497–508 (2016).
42. Manglik, A. *et al.* Structure-based discovery of opioid analgesics with reduced side effects. *Nature* **537**, 185–190 (2016).
43. Váradi, A. *et al.* Mitragynine/Corynantheidine Pseudoindoxyls As Opioid Analgesics with Mu Agonism and Delta Antagonism, Which Do Not Recruit β-Arrestin-2. *J. Med. Chem.* **59**, 8381–8397 (2016).
44. Lodowski, D. T., Pitcher, J. A., Capel, W. D., Lefkowitz, R. J. & Tesmer, J. J. G. Keeping G proteins at bay: a complex between G protein-coupled receptor kinase 2 and Gbetagamma. *Science* **300**, 1256–1262 (2003).
45. DebBurman, S. K. *et al.* Lipid-mediated regulation of G protein-coupled receptor kinases 2 and 3. *J. Biol. Chem.* **270**, 5742–5747 (1995).

46. Kenakin, T. Biased Receptor Signaling in Drug Discovery. *Pharmacol. Rev.* **71**, 267–315 (2019).
47. De Lean, A., Stadel, J. M. & Lefkowitz, R. J. A ternary complex model explains the agonist-specific binding properties of the adenylate cyclase-coupled beta-adrenergic receptor. *J. Biol. Chem.* **255**, 7108–7117 (1980).
48. Sunahara, R. K. & Insel, P. A. The Molecular Pharmacology of G Protein Signaling Then and Now: A Tribute to Alfred G. Gilman. *Mol. Pharmacol.* **89**, 585–592 (2016).
49. Maguire, M. E., Sturgill, T. W., Anderson, H. J., Minna, J. D. & Gilman, A. G. Hormonal control of cyclic AMP metabolism in parental and hybrid somatic cells. *Adv. Cyclic Nucleotide Res.* **5**, 699–718 (1975).
50. Costa-Neto, C. M., Parreiras-E-Silva, L. T. & Bouvier, M. A Pluridimensional View of Biased Agonism. *Mol. Pharmacol.* **90**, 587–595 (2016).